Published online 30 May 2022 *Nucleic Acids Research, 2022, Vol. 50, No. 10* **5919–5933**
https://doi.org/10.1093/nar/gkac431

Cytosolic microRNA-inducible nuclear translocation of Cas9 protein for disease-specific genome modification

Cheol-Hee Shin[1,†], Su Chan Park[2,†], Il-Geun Park[2], Hyerim Kim[3], Byoungha An[1,5], Choongil Lee[1], Sang-Heon Kim[1,5], Juyong Lee[4,*], Ji Min Lee[2,*] and Seung Ja Oh[1,5,*]

[1]Center for Biomaterials, Biomedical Research Institute, Korea Institute of Science and Technology (KIST), Seoul 02792, Republic of Korea, [2]Graduate School of Medical Science & Engineering, Korea Advanced Institute of Science and Technology, 291 Daehak-ro, Yuseong-gu, Daejeon 34141, Republic of Korea, [3]Program in Nanoscience and Technology, Graduate School of Convergence Science and Technology, Seoul National University, Seoul, Republic of Korea, [4]Department of Chemistry, College of Natural Science, Kangwon National University, Chuncheon 24341, Republic of Korea and [5]Division of Bio-Medical Science & Technology, Korea University of Science and Technology (UST), Seoul, Republic of Korea

Received October 20, 2021; Revised May 03, 2022; Editorial Decision May 05, 2022; Accepted May 10, 2022

ABSTRACT

MicroRNA-dependent mRNA decay plays an important role in gene silencing by facilitating posttranscriptional and translational repression. Inspired by this intrinsic nature of microRNA-mediated mRNA cleavage, here, we describe a microRNA-targeting mRNA as a switch platform called mRNA bridge mimetics to regulate the translocation of proteins. We applied the mRNA bridge mimetics platform to Cas9 protein to confer it the ability to translocate into the nucleus via cleavage of the nuclear export signal. This system performed programmed gene editing *in vitro* and *in vivo*. Combinatorial treatment with cisplatin and miR-21-*EZH2* axis-targeting CRISPR Self *Check-In* improved sensitivity to chemotherapeutic drugs *in vivo*. Using the endogenous microRNA-mediated mRNA decay mechanism, our platform is able to remodel a cell's natural biology to allow the entry of precise drugs into the nucleus, devoid of non-specific translocation. The mRNA bridge mimetics strategy is promising for applications in which the reaction must be controlled via intracellular stimuli and modulates Cas9 proteins to ensure safe genome modification in diseased conditions.

INTRODUCTION

MicroRNAs (miRNAs) are 19–24 nucleotide long RNAs that are evolutionarily conserved in animals and play essential roles in post-transcriptional regulation of gene expres-

*To whom correspondence should be addressed. Tel: +82 2 958 5353; Fax: +82 2 958 5308; Email: seungja.oh@kist.re.kr
Correspondence may also be addressed to Ji Min Lee. Tel: +82 42 350 4869; Fax: +82 42 350 4240; Email: jimin.lee@kaist.ac.kr
Correspondence may also be addressed to Juyong Lee. Tel: +82 33 250 8481; Fax: +82 33 259 5667; Email: juyong.lee@kangwon.ac.kr
†The authors wish it to be known that, in their opinion, the first two authors should be regarded as Joint First Authors.
Present addresses:
C.-H. Shin, Center for Biomaterials, Biomedical Research Institute, Korea Institute of Science and Technology (KIST), Seoul 02792, Republic of Korea.
B. An, Center for Biomaterials, Biomedical Research Institute, Korea Institute of Science and Technology (KIST), Seoul 02792, Republic of Korea.
C. Lee, Center for Biomaterials, Biomedical Research Institute, Korea Institute of Science and Technology (KIST), Seoul 02792, Republic of Korea.
S.-H. Kim, Center for Biomaterials, Biomedical Research Institute, Korea Institute of Science and Technology (KIST), Seoul 02792, Republic of Korea.
S.J. Oh, Center for Biomaterials, Biomedical Research Institute, Korea Institute of Science and Technology (KIST), Seoul 02792, Republic of Korea.
S.C. Park, Graduate School of Medical Science & Engineering, Korea Advanced Institute of Science and Technology, 291 Daehak-ro, Yuseong-gu, Daejeon 34141, Republic of Korea.
I.-G. Park, Graduate School of Medical Science & Engineering, Korea Advanced Institute of Science and Technology, 291 Daehak-ro, Yuseong-gu, Daejeon 34141, Republic of Korea.
J.M. Lee, Graduate School of Medical Science & Engineering, Korea Advanced Institute of Science and Technology, 291 Daehak-ro, Yuseong-gu, Daejeon 34141, Republic of Korea.
H. Kim, Program in Nanoscience and Technology, Graduate School of Convergence Science and Technology, Seoul National University, Seoul, Republic of Korea.
J. Lee, Department of Chemistry, College of Natural Science, Kangwon National University, Chuncheon 24341, Republic of Korea.
B. An, Division of Bio-Medical Science & Technology, Korea University of Science and Technology (UST), Seoul, Republic of Korea.
S.-H. Kim, Division of Bio-Medical Science & Technology, Korea University of Science and Technology (UST), Seoul, Republic of Korea.
S.J. Oh, Division of Bio-Medical Science & Technology, Korea University of Science and Technology (UST), Seoul, Republic of Korea.

© The Author(s) 2022. Published by Oxford University Press on behalf of Nucleic Acids Research.
This is an Open Access article distributed under the terms of the Creative Commons Attribution-NonCommercial License (http://creativecommons.org/licenses/by-nc/4.0/), which permits non-commercial re-use, distribution, and reproduction in any medium, provided the original work is properly cited. For commercial re-use, please contact journals.permissions@oup.com

sion (1). MiRNAs are loaded into Argonaute (Ago) proteins, which are highly specialized RNA-binding proteins, and form an RNA-induced silencing complex (RISC). This complex pairs with the 3′-untranslated region of the target messenger RNAs (mRNAs) (2). In general, partial base-pairing of the miRNA with a complementary sequence inhibits the translation of target mRNAs, whereas complete base-pairing with complementary sequences causes an Ago-catalysed target mRNA cleavage and degradation, which leads to post-transcriptional repression (3). Aberrant expression of miRNAs in cells has been detected in various diseases (4); it may potentially be used as biomarkers or therapeutic targets. Despite the active development of miRNA-related strategies, the use of the intrinsic nature of miRNA-mediated cleavage as artificial machinery has not been widely explored.

Studies into the role of miRNAs in disease progression and the potential of miRNAs as drug targets have expanded rapidly. In clinical applications, miRNA profiles might be detected as biomarkers of the disease for diagnosis and prognosis (5–7). However, there were obstacles and application limitations of miRNA-based therapeutics and diagnostics such as delivery from outside, off-target effects, toxicity mediation, miRNA-related immunological activation, and dosage determination (8,9). Further, current miRNA diagnostics have limitations in that we could not detect the right range in the right amount which is the exact barrier between disease and normal cells. Beyond the previous role of non-coding RNAs as biomarkers and therapeutic targets, the development of a new miRNA-mediated platform to detect the barrier which distinguishes diseased cells from the normal ones the inside of the innate cells will enable new approaches to treat disease using the cell's own biology, currently unavailable by conventional approaches.

The CRISPR-Cas9 system has been developed as a revolutionary tool for genome modification (10–12). Although it is a successful strategy, Cas9 proteins still need to be optimized for safe and controlled operation in cells. For this purpose, precise genome editing, particularly in specific cells and tissues, is a crucial consideration. Various attempts have been made to meet the requirements of precise genome editing by intrinsic and extrinsic signals (13). Among these strategies, intrinsic stimuli-responsive CRISPR-related proteins facilitate self-control of precise genome editing. Here, we developed the mRNA bridge mimetics platform, which comprises a synthetic complementary strand of miRNA that can be degraded by endogenous miRNA-Ago complexes in the cytoplasm and applied it to Cas9 protein to confer the ability of self-control. The precise programmability of mRNA bridge mimetics enables Cas9 to accomplish Self *Check-In* to the nucleus by sensing the disease-specific miRNA and cleaving off the nucleus export signal (NES) on it (Figure 1A). The CRISPR Self *Check-In* was retained and degraded in the cytoplasm within 24 h if there were no corresponding miRNAs for cleaving off the programmed mRNA bridge mimetics in the cells. Thus, this strategy is especially promising for applications in which disease-independent off-target editing must be minimized.

MATERIALS AND METHODS

Complex structure modelling

The 3D structure of Cas9 was modelled with the Galaxy-Loop method (14) based on the template structure (PDB ID: 6IFO). The single-stranded structures of mRNA1X and mRNA3X were modelled using the Rosetta software suite (15). Based on the predicted secondary structures of RNA strands by the RNAFold server (16), the 3D structures were generated by using the Rna_de_novo program of the Rosetta suite. The 3D conformations were sampled for 5 000 000 cycles that minimizes the Rosetta RNA energy function. The entire structure of the CRISPR Self *Check-In* system was modeled by energy minimization and MD simulations in the presence of two distance restraints between (i) the C-terminal of NES and the 5′-terminal of an RNA strand and (ii) 3′-terminal of an RNA strand and the N-terminal of Cas9. The energy minimization and MD simulations were performed with FACTS implicit solvation model (17) using CHARMM package (18). The input files for the MD simulations were prepared by the CHARMM-GUI server (19). All figures of protein structures were illustrated by ChimeraX (20).

Binding free energy calculation

To estimate the binding affinities of the CRISPR Self *Check-In* system, the molecular dynamics (MD) simulations and the molecular-mechanics/generalized-Born solvent accessible area (MM-GBSA) calculations (21,22) were performed. The energetics of the complex was modelled with the Amber14sb (23) and RNA.OL3 (24) force fields and solvated using the TIP3P water molecules (25) with a padding region of 12 å. The MD simulation of the modelled complex structure of the CRISPR Self *Check-In* system was performed for 200 ns with explicit solvent. All MD simulations were performed with the *pmemd.cuda* program (26) of the Amber20 molecular simulation package (27). After MD simulation was completed, the MM-GBSA calculation was performed, which is commonly used to estimate the binding affinities of protein-ligand, protein-protein, and protein-nucleic acid complexes. The MM-GBSA calculation was performed with the *MMPBSA.py* program of the AmberTools20 package (28). From the trajectory of 200 ns of MD simulations, a total of 500 snapshots were sampled for every 0.4 ns to calculate the energetics of the complex formation. The solvation energies were evaluated with the modified GB model, igb = 5 (29).

Construction of mRNA bridge mimetics

In order to conjugate the NES (Nuclear Export Signal, LDLASLIL) peptide with the miRNA target oligo, either DBCO or Azido were synthesized on the NES peptide. NES (N)- DBCO, NES (C)- DBCO, NES (N) - Azido, and NES (C)- Azido peptides were synthesized, but NES (N)- DBCO was not able to be obtained. The synthesis was confirmed using a Shiseido capcell pak C18, 5 μm, 120 Å (4.6 × 50 mm) column with SHIMADZU Prominence HPLC and mass analysis with SHIMADZU LCMS-2020.

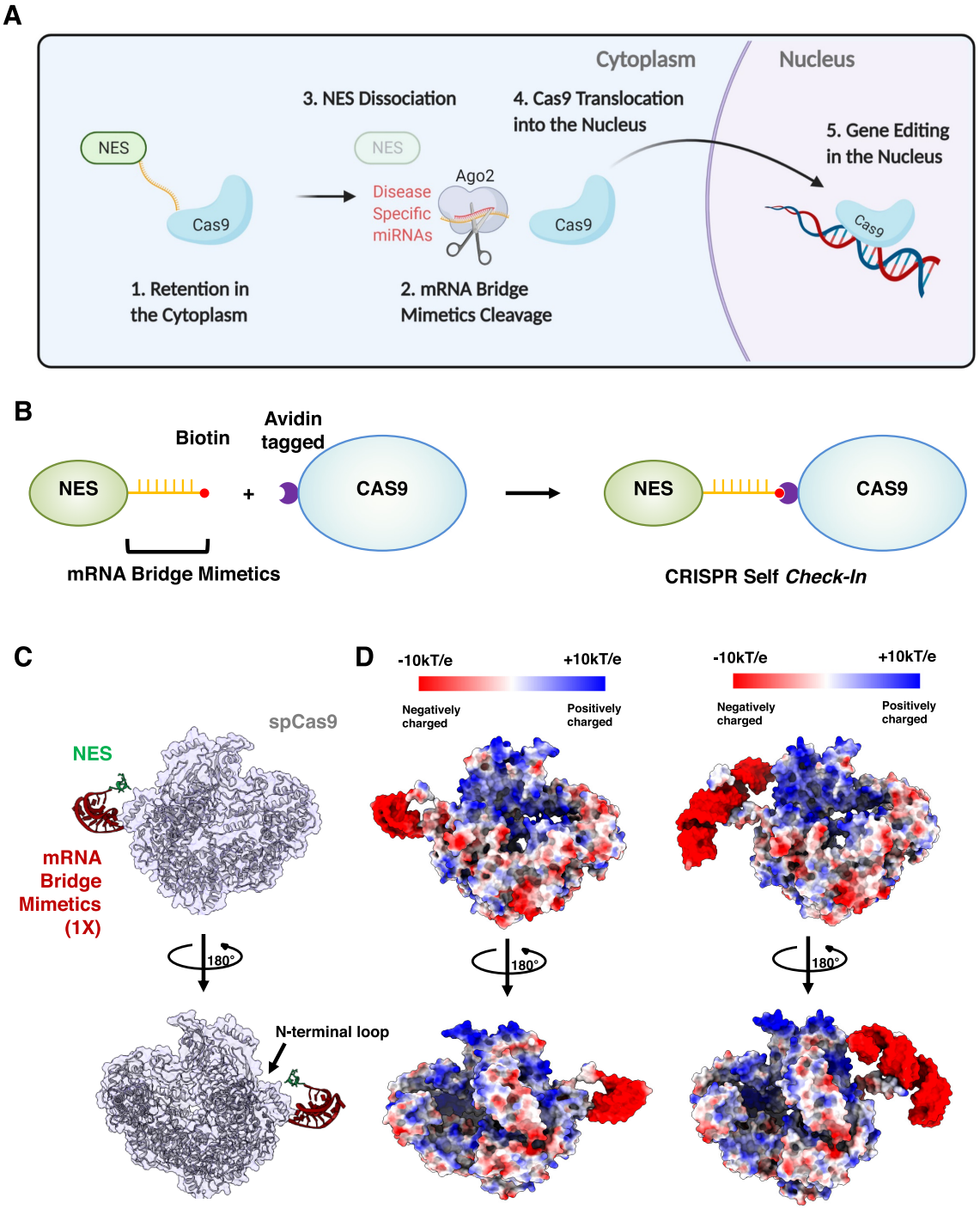

Figure 1. mRNA bridge mimetics for the programmed cleavage by Ago-catalyzed miRNA-mediated mRNA decay and its application to control nucleus translocation of CRISPR Self *Check-In*. (**A**) Schematic representation of CRISPR Self *Check-In* operation for controlled genome editing. In disease cells, CRISPR Self *Check-In* controls nucleus translocation of Cas9 proteins for disease-specific genome editing by sensing miRNAs and being cleaved off mRNA bridge mimetics containing NES. (**B**) Design of CRISPR Self *Check-In*. CRISPR Self *Check-In* is a ribonucleoprotein (RNP) composed of a Cas9 endonuclease and mRNA bridge mimetics containing NES. mRNA bridge mimetics binds to the recombinant Cas9 protein by biotin–avidin interaction. Yellow: mRNA bridge mimetics, Red: Biotin, Purple: Avidin tagged. (**C**) Surface representation of the modelled CRISPR Self *Check-In* (**D**) Surface electrostatic potential maps of modelled CRISPR Self *Check-In* with mRNA1X (left) and mRNA3X (right) are depicted colored from −10 kT/e (red) to +10 kT/e (blue).

mRNA bridge mimetics with the complete complementary sequence of either hsa-miR-21-5p or mmu-miR-294-3p miRNA were synthesized and modified by either azide or DBCO at the 5′ end and biotinylated at the 3′ end on a 100 nm scale through Integrated DNA Technologies (IDT). HPLC Purification was performed. Modified NES and the mRNA bridge mimetics were conjugated via DBCO and azide click reaction. The binding was confirmed by BCA analysis using a biotin pull-down assay using Dynabeads™ M-280 Streptavidin (Thermo Fisher Scientific, 11205D).

Reporter constructs and luciferase assay

The complete complementary sequence of target miRNA was inserted in multiple cloning regions of psiCHECK™-2 Vector (Promega, #C8021) using restriction enzyme Xho1 and EcoR1. The recombined miRNA target-psiCHECK™-2 vector was transfected into HeLa cells using Lipofectamine™ 2000 Transfection Reagent (Invitrogen). After 48 h, the luciferase activity was expressed by the Dual-Luciferase® Reporter Assay System (Promega, #E1910) and measured using the GloMax-Multi Detection System (Promega) (30).

Purification of the Cas9 fusion protein

pET-Cas9-NLS-6xHis plasmids were transformed into *Escherichia coli* BL21 (DE3) competent cells, and incubated overnight at 37°C using Luria-Bertani agar plates containing ampicillin (100 μg/ml) as described previously (31). The transfected BL21 cells were selected and cultured overnight at 120 rpm at 20°C in 3L of LB-ampicillin broth with 1 mM isopropyl-β-D-thiogalactopyranoside (IPTG). Cells were collected by ultra-centrifugation and lysed with lysis buffer (50 mM NaH_2PO_4, 300 mM NaCl, 5 mM imidazole (pH8.0)). After ultra-centrifugation at 18 000 rpm for 40 min at 4°C, the soluble lysate was incubated at Ni-NTA resin (Thermo Fisher Scientific) for 2 h at 4°C. After washing with washing buffer (50 mM NaH_2PO_4, 300 mM NaCl, 20 mM imidazole) (pH 8.0)), it was eluted with elution buffer (50 mM NaH_2PO_4, 300 mM NaCl, 100 mM imidazole (pH 8.0), 50 mM NaH_2PO_4, 300 mM NaCl, 250 mM imidazole (pH 8.0)). After concentration, the buffer was changed with PBS. The purity of the Cas9 protein was confirmed by coomassie blue SDS-PAGE gel staining.

Confirmation of CRISPR Self *Check-In*

EGFP sgRNA targeting GFP (GAAGTTCGAGGGCG ACACCC) was synthesized by Integrated DNA Technologies (IDT) Alt-R® CRISPR-Cas9 sgRNA at 10 nm scale. To generate Cas9 RNPs, Cas9 protein and EGFP sgRNA were incubated in PBS buffer for 30 min at 37°C as described previously (31). EGFP targeting Cas9 RNP transfected into the GFP stable HeLa cell line using Neon® Transfection System (Thermo Fisher Scientific) or Lipofectamine™ CRISPRMAX™ Cas9 Transfection Reagent (Invitrogen) (32). The function of Cas9 fusion protein was confirmed by In Vitro Cleavage (IVC) test, T7E1 assay, confocal microscope and western blot analysis.

RT-qPCR

The total RNA was extracted using TRIzol reagent (Invitrogen, Cat#15596018). The cDNA was amplified and quantified using SYBR Premix Ex Taq (Takara, #RR420L) with the following primers: EZH2_F: 5′-CCC TGA CCT CTG TCT TAC TTG TGG A -3′, EZH2_R: 5′-ACG TCA GAT GGT GCC AGC AAT A -3′, KRAS_F: 5′-CAGTAGACACAAAACAGGCTCAG-3′, KRAS_R 3′-TGTCGGATCTCCCTCACCAATG-5′, GAPDH_F: 5′-GTC AGT GGT GGA CCT GAC CT-3′, GAPDH_R: 5′-AAA GGT GGA GGA GTG GGT GT-3′. Real-time PCR was performed using the Applied Biosystems 7500 real-time cyclers as described previously (17).

Western blot

Antibodies specific for Cas9 (sc-517386), His (sc-8036), GFP (SC-9996) were purchased from Santa Cruz Biotechnology and EZH2 (3147), ERK (9102), pERK (9101) were purchased from Cell Signaling Technology. The images were obtained using an iBright Western Blot Imaging System (Thermo Fisher Scientific).

MicroRNA isolation, MicroRNA cDNA synthesis, MicroRNA RT-qPCR and MicroRNA inhibitors

MicroRNA was extracted using RNAzol RT (Sigma, Cat#R4533) as described previously (17). After isolation, microRNA was converted into cDNA templates using the MystiCq miRNA cDNA Synthesis Mix Kit (Sigma, Cat#MIRRT). The amplification of miRNA cDNAs was quantified in real-time SYBR Green RT-qPCR reactions using a MystiCq miRNA Universal PCR Primer and individual MystiCq miRNA qPCR Assay Primer by the Applied Biosystems 7500 real-time cyclers (Applied Biosystems). AccuTarget™ Human miRNA-21 Inhibitor (Bioneer, #MI0000077), a single-stranded synthetic inhibitor with a complementary sequence to target human microRNA, was used in miRNA loss-of-function studies.

Human cell lines

Human cancer cell lines (HeLa, Calu-3, H827, A549, H358, H1299, MCF-10A, MDA-MB-231, BT-20, HCC1937 and MCF7) were purchased from the American Type Culture Collection (ATCC) and maintained in EMEM supplemented with 10% FBS (GIBCO BRL) at 37°C in a humidified atmosphere with 5% CO_2 as described previously (33). GFP stable sublines of HeLa were selected by G418. All cell lines were authenticated by the ATCC and were consistent with their presumptive identity.

Immunohistochemistry (IHC)

For the IHC, the tumors were fixed in 4% paraformaldehyde overnight, embedded in paraffin. The tumor sections were incubated with anti-EZH2 (Thermofisher, Catalog #36-6300) primary antibodies in the blocking solution at 4°C overnight as described previously (17). For the secondary antibody, HRP-labeled anti-rabbit IgG (Cell Signaling Technology, #31460) was incubated at room tem-

perature for 1 h. The samples were reacted with a 3,3′-diaminobenzidine (DAB) kit (Vector Labs, sk-4100).

Immunofluorescence

For immunofluorescence staining, cells were seeded in eight-well slides (Ibidi #80826) with 104 cells/500 μl. mRNA bridge mimetics platform was formed in three steps. Firstly, 6 μl of NES-DBCO (100 μM) was conjugated with 2 μl of Azido-Oligo (100 μM) for 30 min at 37°C. Secondly, NES oligo complex was fused with 0.6 μl of Cas9 (0.5 μg/μl) overnight at 4°C. Finally, NES-oligo-Cas9 fusion protein was combined with 1.2 μl of sgRNA (0.1 μg/μl) for 30 min at 37°C. Lipofectamine CRISPRMAX was mixed with Cas9 complex (ThermoFisher #CMAX0008) for cell transfection, and 25 μl/well of complete form was treated to cells. To measure the nuclear translocation of Cas9 RNP, immunoreaction was performed with anti-His (Abcam, ab18184) for Cas9 and anti-Flag (Sigma, F7425) for Ago2 in 3% (w/v) BSA solution at 4°C overnight. After washing, the samples were incubated for 1 h at room temperature with Alexa Fluor 488 goat anti-mouse IgG (Invitrogen, A11001; 1:100) and Alexa Fluor 594 donkey anti-rabbit IgG (Invitrogen, A21207; 1:100) as described previously (17). pCK-Flag-Ago2 was transfected with A549 cells 48 h before CRISPR Self *Check-In* system transfection, for immunostaining *in vivo*, the tumor sections were incubated with anti-EZH2 (Cell Signaling Technology, # 3147S) and detected by Alexa Fluor 488 goat anti-mouse IgG (Invitrogen, A11001; 1:100). The sections were mounted with DAPI mounting medium (Vector, H-1200). The fluorescent signals were visualized using a confocal microscope (Carl Zeiss, LSM700).

Viability assay

The cell viability was measured using CellTiter-Glo Luminescent Cell Viability Assay (Promega, Cat#G7570) by GloMax Discover Multimode Microplate Reader (Promega).

T7E1 assay

Genomic DNA was extracted using the G-DEX IIc Genomic DNA Extraction Kit (iNtRON) after 3 days of transfection. Cas9 target sites were PCR amplified using primer pairs listed below. The amplicons were denatured by heating and annealed to form heteroduplex DNA, which was treated with 5 units of T7 endonuclease 1 (New England Biolabs, Ipswich, MA) for 20 min at 37°C and then analyzed by 2.5% agarose gel electrophoresis. EZH2_ t7e1_F: 5′- GCT TAT TGG TGA GAG GGG TCT -3′, EZH2_ t7e1_R: 5′- GTG GCA AAC ATG ATC CTC CT -3′, EZH2_ long_F: 5′- TAT ATG CCA CAG AAG CAG AGC C -3′, EZH2_ long_R: 5′- TCC CAA ACT CCA CTT GAT GAT CC -3′, EZH2_ short_F: 5′- GCC CAG GTT CAG TCC CTT ATA G -3′, EZH2_ short _R: 5′- GCT TAT TGG TGA GAG GGG TCT -3′.

Targeted deep sequencing

Genomic DNA segments that encompass the nuclease target sites were amplified using Phusion polymerase (New England Biolabs). Equal amounts of the PCR amplicons were subjected to paired-end read sequencing using Illumina MiSeq. Rare sequence reads that constituted <0.005% of the total reads were excluded. Rates of insertions or deletions were analyzed by Cas-Analyzer (34).

Animal study

Five-week-old immunodeficient nude mice (nu/nu) mice (Orient Bio) were maintained in pressurized ventilated cages. For *ex vivo* xenograft, A549 cells were transfected with Cas9 RNPs using Lipofectamine CRISPRMAX™ Cas9 Transfection Reagent (Invitrogen) *in vitro* and the A549 cells (1×10^7) were injected subcutaneously into mice after 24 h of the transfection. For *in vivo* xenograft, A549 cells (1×10^7) were injected subcutaneously into mice and Cisplatin and/or Cas9 RNPs using Lipofectamine CRISPRMAX™ were administered by intratumoral injection after 14 days of the inoculation. Tumor response was regularly monitored every 4 days after treatment. Tumor volume was measured at the beginning of treatment and then monitored regularly. Tumor volume (V) was calculated by using the following modified ellipsoidal formula: $V = 0.5 \times \text{length} \times (\text{width})^2$ as described previously (33). All studies were performed with the approval of the Animal Care and Use Committee of the Korea Institute of Science and Technology and Korea Animal Protection Law.

Statistical analysis

All numerical values are presented as means ± standard deviation (SD). Statistical analyses were performed using GraphPad Prism 8.4.3. A P-value of less than 0.05 was considered statistically significant.

RESULTS

mRNA bridge mimetics and its therapeutic application in Cas9 protein, CRISPR Self *Check-In*

CRISPR Self *Check-In* is a ribonucleoprotein (RNP) composed of a Cas9 endonuclease and mRNA bridge mimetics containing an NES (Figure 1B). To predict the structure of CRISPR Self *Check-In*, we modelled the structures of Cas9-mRNA bridge mimetics 1X repeat-NES (CRISPR Self *Check-In* 1X) and Cas9-mRNA bridge mimetics 3X repeats-NES (CRISPR Self *Check-In* 3X). The N-terminal region of our Cas9 system, from the Met1 to His14 residue, forms a helix and is extruded out from the main Cas9 domain via a flexible loop, which ranges from the Glu15 to Lys19 residue (Figure 1C and D). Thus, the coupled mRNA bridge mimetics were almost completely exposed to the solvent, which allowed a complementary miRNA strand to approach and recognize the mRNA bridge mimetics. The unpaired mRNA bridge mimetics were predicted to form twisted helical structures. The electrostatic maps show that the mRNA structure is highly negatively charged, whereas

the groove of Cas9 is highly positively charged (Figure 1D). In both modelled structures, the NES peptides are completely exposed to the solvent. This suggests that the unpaired strands and the NES peptide are recognizable and fully functional in the cytoplasm.

mRNA bridge mimetics for Cas9 protein

In the design of CRISPR Self *Check-In*, the translocation of Cas9 into the nucleus is programmed by mRNA bridge mimetics. In CRISPR Self *Check-In*, the avidin tagged Cas9 interacts with the biotinylated mRNA bridge mimetics. For the experiment, an NES peptide modified by either dibenzocyclooctyne (DBCO) or azide at the N- or C-terminus was synthesized and confirmed by high-performance liquid chromatography and mass spectrometry analysis (Figure 2A and Supplementary Figure S1). The miR-21 expression has been shown in many diseases including cancers (35–40). Therefore, the 1X or 3X repeated complementary sequence of human miRNA hsa-miR-21-5p (H1X or H3X) for disease cells and mouse miRNA mmu-miR-294-3p (M1X or M3X) as negative controls were tested as mRNA bridge mimetics (Table S1). The oligonucleotide was synthesized with the completely complementary sequence of miRNAs and modified by either azide or DBCO at the 5′ end and biotinylated at the 3′ end. Next, we confirmed the reaction between the NES peptide and the oligonucleotide by a pull-down assay with streptavidin beads. Then, the yield was measured by sodium dodecyl sulfate-polyacrylamide gel electrophoresis and bicinchoninic acid assay. As shown in Figure 2B and Supplementary Figure S2a, the highest yield of the reaction was obtained from the NES peptide modified at the C-terminus with DBCO, and 3X repeats of miRNA cleavable oligonucleotides. To confirm the cleavage of the mRNA bridge mimetics, a single-stranded RNA (ssRNA) reporter with the same sequence of H1X was synthesized, and the intensity of the fluorescence emitted by the cleaved reporter was measured (Figure 2C). The cleavage of mRNA bridge mimetics was increased with the dose of miRNA mimics in a time-dependent manner in A549 cells. To confirm the versatility of the mRNA bridge mimetics, a single-stranded RNA (ssRNA) reporter with a complementary sequence of human miRNA hsa-miR-19a-5p was also synthesized. Fluorescence following the cleavage of the mRNA bridge mimetics by miR-19a mimics increases in a dose and time-dependent manner in A549 cells (Supplementary Figure S2b). The specificity of the cleavage of mRNA bridge mimetics was also tested using a recombinant plasmid containing the complementary sequence of either miR-21 or miR-294. A luciferase assay was performed to quantify the cleavage after the construct was transfected into HeLa cells (41), which express high levels of miR-21 and not miR-294 (Figure 2D and Supplementary Figure S2c). The decreased luciferase activity mediated by miR-21 was observed for H1X and H3X but not for M1X and M3X, indicating that the designed miRNA complementary oligonucleotides exhibited target specificity. Additionally, we also observed that the stability of oligonucleotides was decreased with the increasing number of oligonucleotide repeats (Figure 2D and Supplementary Figure S2b). The cumulative luciferase activity of CON, M1X, and M3X was detected for up to 72 h (Figure 2E).

For the endonuclease function, the Cas9 was cloned and prepared for interaction with the biotinylated mRNA bridge mimetics (Supplementary Figure S3a and b). As shown in Figure 2F, the expression of Cas9 was confirmed after transfection into HeLa cells by a pull-down assay. We also observed that approximately 90% of the Cas9 was degraded in 24 h after transfection into the cells (Figure 2G and H). Finally, the Cas9 protein was able to knock out green fluorescent protein (GFP) in GFP-stable HeLa cells (Figure 2I and J) (32). Together, the function of mRNA bridge mimetics combined with Cas9 as components of CRISPR Self *Check-In* were confirmed.

mRNA bridge mimetics controls CRISPR Self *Check-In* translocation into the nucleus by cytosolic miRNAs

CRISPR Self *Check-In* is a newly designed RNP composed of Cas9 endonuclease and mRNA bridge mimetics. The mRNA bridge mimetics programmed for the cleavage only triggered by miR-21 (N-H1X or N-H3X) was first assembled as CRISPR Self *Check-In* for genome modification in GFP-stable HeLa cells. As expected, only N-H1X and N-H3X programmed CRISPR Self *Check-In*-targeting GFP was able to knock out GFP after transfection using Lipofectamine™ CRISPRMAX™ Cas9 Transfection Reagent (Invitrogen) in the GFP-stable HeLa cells (Figure 3A and B). In contrast, for N-M1X and N-M3X, the CRISPR Self *Check-In*s programmed for activation by mouse miR-294 were not able to knock out GFP, indicating the controlled activation of CRISPR Self *Check-In*. Consistent with this data, the programmability of CRISPR Self *Check-In* for controlled genome modification was also confirmed by a biochemical assay (Figure 3C and D).

To prove the hypothesis that CRISPR Self *Check-In* translocates into the nucleus for genome editing when the mRNA bridge mimetics containing the NES peptide is cleaved off by the complementary miRNA, we traced the localization of CRISPR Self *Check-In* programmed for miR-21 after transfection using Lipofectamine™ CRISPRMAX™ Cas9 Transfection Reagent (Invitrogen) into A549 cells. As shown in Figure 3E and F, the conventional Cas9 was translocated into the nucleus in 3 h, whereas the translocation of N-H1X was completed in 12 h. As expected, the N-M1X-Cas9 programmed for mouse microRNA-294 was not able to translocate into the nucleus. The translocated CRISPR Self *Check-In* was degraded within 24 h (Supplementary Figure S4).

Additionally, we confirmed the specificity of the cleavage of mRNA bridge mimetics in CRISPR Self *Check-In* by testing other miRNAs with different levels of expression in A549 cells. The miR-19a and miR-21 expressed at low and high levels in HeLa cells, respectively, were confirmed by both miRNA quantitative PCR and luciferase miRNA activity assay (Figure 3G and H). To test its specificity in translocation and gene editing, the CRISPR Self *Check-In* programmed for miR-19a and miR-21 were transfected with sgRNA-targeting GFP in GFP-stable HeLa cells. Only CRISPR Self *Check-In* programmed for translocation by miR-21 was able to knock out GFP, confirming both the specificity and programmability of the function of mRNA bridge mimetics (Figure 3I). The mRNA bridge mimetics

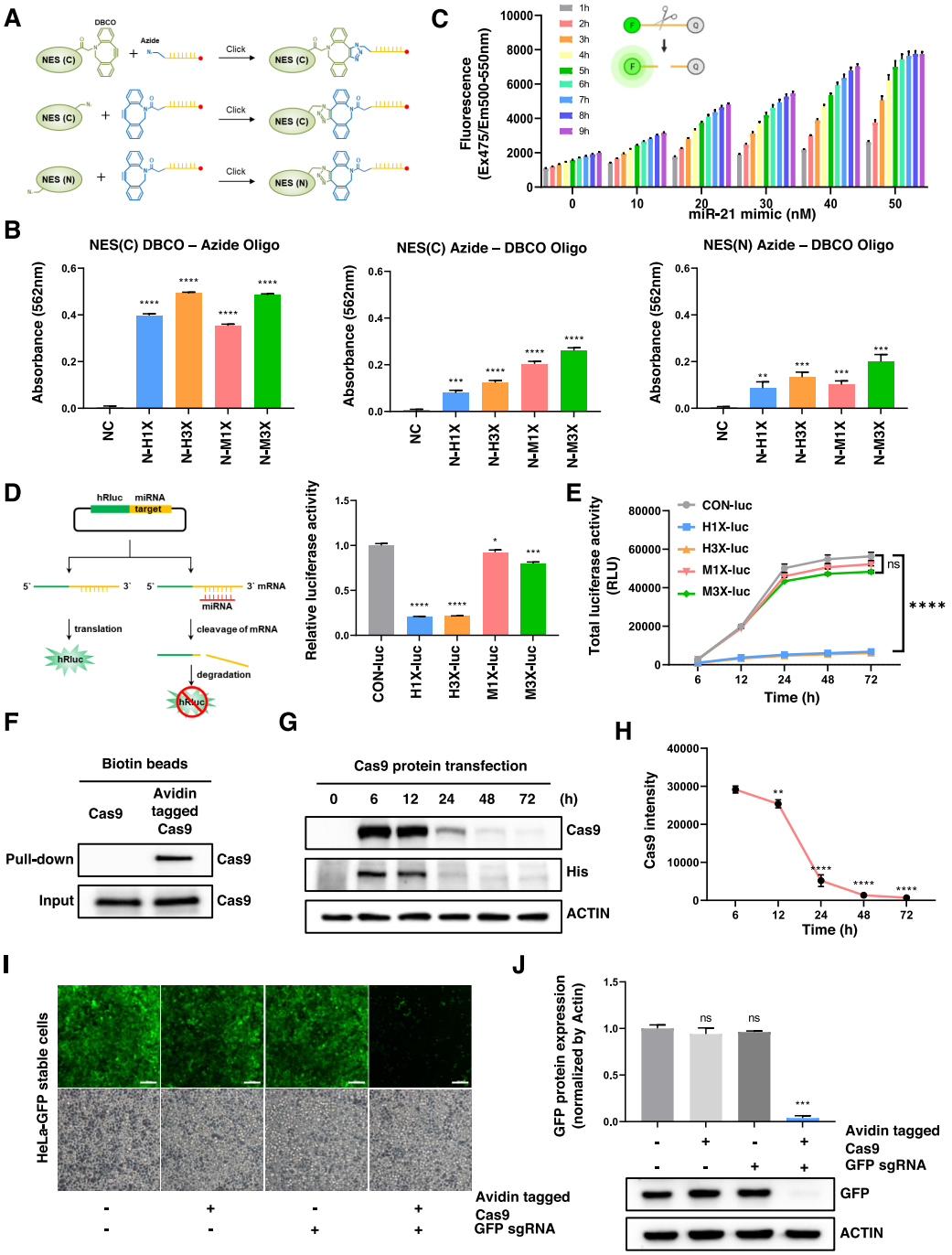

Figure 2. mRNA bridge mimetics for CRISPR Self *Check-In*. (**A**) The reaction between NES and mRNA bridge mimetics via click chemistry of dibenzocyclooctyne (DBCO) and azide. NES (N)-DBCO was not synthesized. (**B**) The yield of the reaction between NES and mRNA bridge mimetics was evaluated by BCA assay via streptavidin pull-down using biotin from mRNA bridge mimetics. NC: Negative control, N-H1X: NES conjugated oligonucleotides which present a Human miR-21 target site 1X, N-H3X: NES conjugated oligonucleotides which present a Human miR-21 target site 3X, N-M1X: NES conjugated oligonucleotides which present a Mouse miR-294 target site 1X, N-M3X: NES conjugated oligonucleotides which present a Mouse miR-294 target site 3X. Sequences are provided in Supplemental Table S1. (**C**) Fluorescence following the cleavage of the mRNA bridge mimetics by miRNA mimics increases in a dose- and time-dependent manner in A549 cells. The N- and C- terminus of mRNA bridge mimetics were modified by the FAM reporter-dye (F) and the Iowa Black quencher (Q), respectively. λex = 475 nm, λem = 500-550 nm. (**D**) The cleavage specificity of mRNA bridge mimetics are verified through recombinant luciferase vector including human miRNA target sequence. After 24 h of the vector transfection into HeLa cells, the luciferase activity was measured for each construct. (**E**) The luciferase activity was measured and summed up to each point to show the total cleavage of mRNA bridge mimetics by the time. (**F**) The functionality of the recombinant Cas9 proteins was confirmed by biotin beads pull-down assay. (**G**) Most of the Cas9 recombinant proteins were degraded in HeLa cells within 24 h after the transfection. (**H**) Quantification of Cas9 signal intensity normalized by actin in (G). (**I and J**) Nuclease activity of the Cas9 was confirmed by reducing GFP protein expression in HeLa GFP stable cells. Bars indicated 100 μm. All experiments in the present study were performed in triplicate. Error bars represent SD over biological replicates. *P* values were obtained using One-way ANOVA. ns; no statistical significance, $^{**}P < 0.01$, $^{***}P < 0.001$ and $^{****}P < 0.0001$.

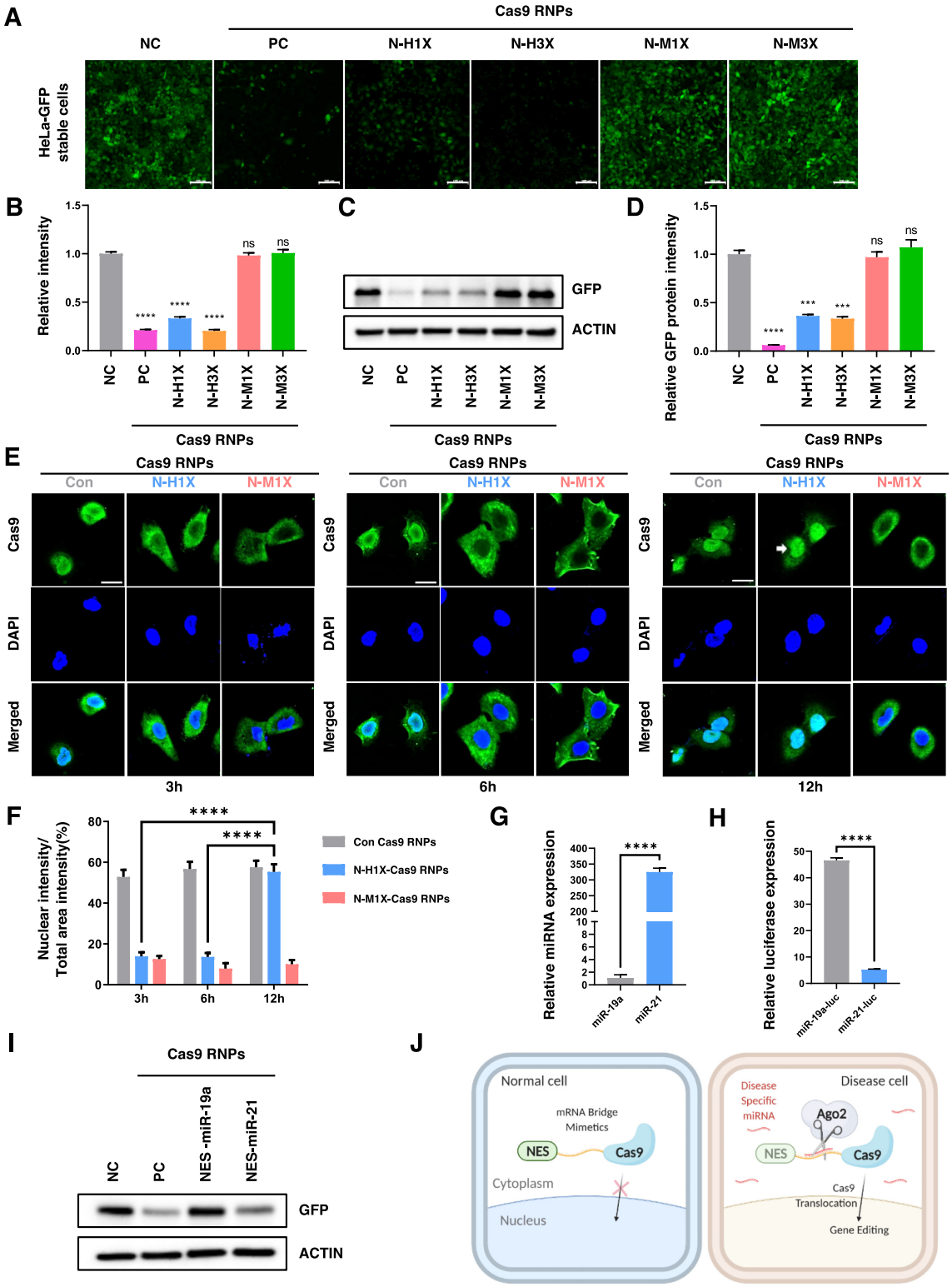

Figure 3. mRNA bridge mimetics to control translocation of CRISPR Self *Check-In* into the nucleus by miRNAs. (**A**, **C**) Knock-out of GFP by Cas9 (PC) or CRISPR Self *Check-In* (N-H1X and N-H3X) was observed in HeLa-GFP stable cells expressing miR-21, not miR-294 after 24 h of the transfection. Green = GFP protein, Bars indicated 100 μm. (**B**, **D**) The relative signal intensity of GFP in (A) and (C) normalized by actin respectively. (**E**) Nuclear translocation was observed in A549 cells after the Cas9 protein (Con) or the CRISPR Self *Check-In* (N-H1X) transfection and the fixation at 12 h. Arrow indicates the translocation of Cas9 into the nucleus. Bars indicated 20 μm. (**F**) The quantification of nuclear translocation from (E). (**G**) Relative miR-19a and miR-21 expression in HeLa-GFP stable cells. (**H**) The cleavage of mRNA bridge mimetics measured by luciferase expression in HeLa-GFP stable cells. (**I**) Knock-out of GFP by CRISPR Self *Check-In* triggered by human miR-21 in HeLa-GFP stable cells. (**J**) Schematics of the disease-specific operation of CRISPR Self *Check-In*. All experiments in the present study were performed in triplicate. Error bars represent SD over biological replicates. *P* values were obtained using unpaired Student's *t*-test. ns; no statistical significance, ***$P < 0.001$ and ****$P < 0.0001$.

integrated CRISPR Self *Check-In* RNP was capable of directing translocation into the nucleus by cytosolic miRNAs. The ability of CRISPR Self *Check-In* for controlled genome modification was also confirmed (Figure 3J).

Ago-dependent mechanism of mRNA bridge mimetics and CRISPR Self *Check-In* operation

Loading miRNAs into the Ago protein to form a RISC is essential for its pairing with target mRNAs for cleavage. To test the Ago dependency of mRNA bridge mimetics, we first confirmed the co-localization of Ago2 and CRISPR Self *Check-In* in the cytoplasm after the transfection of the platform in Ago2-overexpressing A549 cells. Ago2 was shown to coexist in the cytoplasm with CRISPR Self *Check-In* 6 h after transfection (Figure 4A). Interestingly, we observed that N-H1X-Cas9 RNP was localized both in the cytoplasm and nucleus, whereas N-M1X-Cas9 RNPs were only localized in the cytoplasm 6 h after transfection, indicating selective translocation of CRISPR Self *Check-In* by specific miRNAs. Furthermore, we also noticed that the translocation of N-H1X-Cas9 RNPs programmed for miR-21 into the nucleus occurred in 6 h, whereas it took 12 h in A549 cells that do not overexpress Ago2, implicating the accelerated cleavage of mRNA bridge mimetics by Ago2. The translocation of CRISPR Self *Check-In* was even shown 3 h after the transfection in Ago2 overexpressing-A549 cells, which strongly supported the Ago2-dependent mechanism of CRISPR Self *Check-In* (Figures 3E and 4B). Next, we modelled the structures of the CRISPR Self *Check-In*:miRNA-Ago complex (Figure 4C). The modelled structure revealed that the attachment of human Ago2 is possible in CRISPR Self *Check-In* despite the existence of a large Cas9 domain. The double-helical structure of the mRNA and miRNA duplex may protrude from the Cas9 domain. The modelled structure of Ago2 and the RNA double helix clearly showed that the Ago2 domain is readily accessible to the RNA duplex without significant hindrance by Cas9, suggesting that Ago2 is able to cleave the target mRNA. Additionally, the existence of NES does not hinder the binding of Ago2 to the RNA double helix.

To confirm these Ago-dependent mechanics further, the binding affinity between CRISPR Self *Check-In* and Ago2 was estimated with MD simulations and MM-GBSA calculations. The binding affinity between CRISPR Self *Check-In* and Ago2 was estimated to be –400.3 kcal/mol indicating that they would form strong attractive interactions spontaneously. The large absolute value of binding affinity is a well-known limitation of MM-GBSA that overestimates the electrostatic interactions between proteins and nucleic acids. However, a large-scale benchmark study shows that the results of MM-GBSA calculations are well-correlated with experimental pK_d values. The protein-RNA complex systems whose binding affinities are greater than –300 kcal/mol have higher pK_d values than 10.0 in general (42).

mRNA bridge mimetics as a novel switch platform for controlled genome editing of CRISPR Self *Check-In*

mRNA bridge mimetics utilized the aberrant expression of miRNAs, commonly observed in disease conditions, as an intracellular trigger to direct translocation of CRISPR Self *Check-In* into the nucleus for controlled gene editing. Modulation of miR-21 expression has been shown in many diseases including cancers (35–40). Among the underlying mechanism associated with miR-21 regulation, ELK1 has been shown to activate miR-21 transcription by direct binding to the miRNA proximal promoter region, thereby involved in lung tumorigenesis (37). In addition, MEK-ERK1/2-Elk-1 pathway leads to a well-known oncogene, *EZH2*, overexpression in breast cancer cells (43). Therefore, we hypothesized that miR-21 may regulate EZH2 expression in cancers. First, we checked the expression of an oncogenic miRNA, miR-21, which is detected in human cancers and several lung and breast cancer cell lines (Figure 5A). Consistent with the previous report, the cells with high miR-21 expression showed the enhanced expression of a well-known oncogene, *EZH2*, in cancer cells (Figure 5A) (39). Also, we observed that *EZH2* mRNA expression increased in a dose-dependent manner when a miR-21 mimic was transfected in A549 cells (Figure 5B). We also confirmed a dose-dependent decrease in EZH2 expression when miR-21 specific inhibitors were transfected in A549 cells (Figure 5C, S5a and b). KRAS has been considered one of the most promising targets in non-small cell lung cancer (NSCLC). It has been shown that miR-21 expression is significantly enhanced in NSCLC and KRAS induces lung tumorigenesis through miR-21 modulation (37). Also, overexpression of miR-21 leads to enhances KRAS-mediated lung tumorigenesis, whereas genetic deletion of miR-21 partially protects against tumorigenesis (44). We compared the *KRAS* mRNA and miR-21 expression in lung and breast cancer cells and found that the cells with high miR-21 expression tend to show enhanced mRNA expression of *KRAS* (Figure 5D). After then, we confirmed that CRISPR Self *Check-In* targeting KRAS using mRNA bridge mimetics cleavable by miR-21 (NH-1X) is able to knockout KRAS while CRISPR Self *Check-In* targeting KRAS using mRNA bridge mimetics cleavable by miR-294 (NM-1X) fails to knockout KRAS in A549 cells (Figure 5E). Through these results, we confirmed that CRISPR Self *Check-In* can target miR-21-KRAS pair and also be possibly applicable to different combinations of miR-target gene pairs. To analyse controlled gene editing by miRNA expression, we selected Calu-3, A549, and H1299 cells as representatives of cells expressing miR-21 at low, medium, and high levels, respectively. Next, we checked the rates of nuclear translocation of CRISPR Self *Check-In* by miR-21 using Lipofectamine™ CRISPRMAX™ Cas9 Transfection Reagent (Invitrogen). After we confirmed the delivery efficiency of Cas9 protein in Calu-3, A549, and H1299 cells, we found that no translocation of CRISPR Self *Check-In* was observed in Calu-3 cells with low miR-21 expression for up to 12 h (Supplementary Figures S6, 5F and G). However, the nuclear translocation was detected at 12 h after the transfection in A549 cells with medium expression of miR-21 and at 6 h with the high expression of miR-21 after the transfection in H1299 cells. This result demonstrated the miRNA level-based control of CRISPR Self *Check-In* translocation. Consistent with the data showing miRNA expression-dependent translocation, CRISPR Self *Check-In* also showed miRNA expression-dependent gene editing (Figure 5F–I, Supplementary Figure S3c and d).

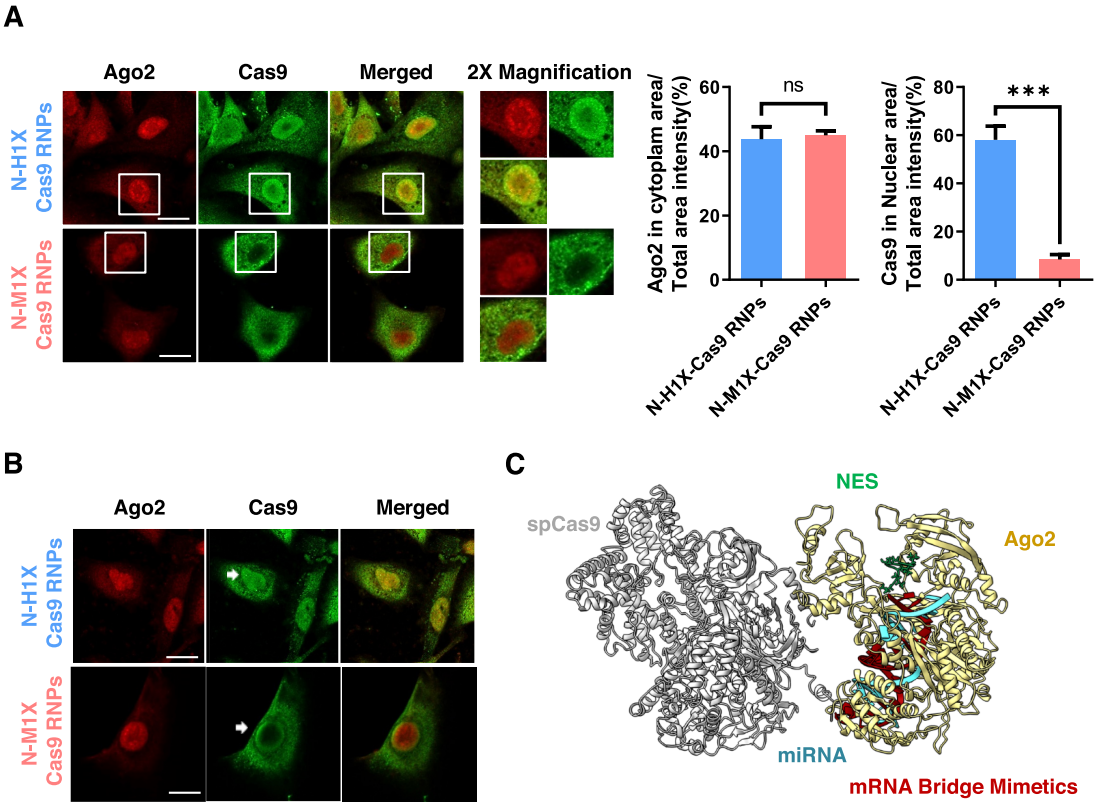

Figure 4. Ago-dependent operation of mRNA bridge mimetics in CRISPR Self *Check-In*. (**A**) Co-localization of Ago2 and CRISPR Self *Check-In* in the cytoplasm and programmed nuclear translocation of Cas9 RNPs triggered by endogenous human miR-21 6 h after the transfection in A549 cells. 2X Magnification = 2X Magnification of the squares enclosed the nucleus. (**B**) Accelerated nuclear translocation of CRISPR Self *Check-In* by the exogenous expression of Ago2 observed 3 h after the transfection in A549 cells. Arrow indicates induced translocation of Cas9 into the nucleus using N-H1X by miRNA-21 (Top) and no translocation of Cas9 into the nucleus using N-M1X (Bottom). Bars indicated 20 μm. (**C**) The model structure of the CRISPR Self *Check-In*:miRNA-Ago2 complex. The Ago2 protein is shown in yellow. The mRNA and miRNA are shown in red and blue, respectively. The Cas9 protein is shown in gray and the NES peptide is shown in green. All experiments in the present study were performed in triplicate. Error bars represent SD over biological replicates. *P* values were obtained using unpaired Student's t-test. ns; no statistical significance, ***$P < 0.001$.

The potential of mRNA bridge mimetics in therapeutic applications

Finally, the potential of mRNA bridge mimetics in therapeutic applications was tested by the controlled gene editing of CRISPR Self *Check-In* and its biological effects in lung cancer cells *in vitro*. *EZH2*-targeting CRISPR Self *Check-In* decreased cancer cell viability by inhibition of ERK signaling pathway (Figure 6A and B). The knock-out of *EZH2* was also well-controlled, as evidenced by the selective gene editing with CRISPR Self *Check-In* programmed for human miR-21 and not with that for mouse miR-294 (Figure 6B and C). The potential of CRISPR Self *Check-In* to be employed for anti-cancer therapeutics was explored by determining the anti-tumour efficacy of *EZH2*-targeting CRISPR Self *Check-In* via selective gene editing *in vivo* (Figure 6D–F). Only the cancer cells treated with *EZH2*-targeting CRISPR Self *Check-In* by the human miR-21, and not mouse miR-294, showed the decreased tumorigenic potential compared to the cells treated with control in A549 lung cancer xenograft (Figure 6A–F). The precise gene-editing system and its therapeutic efficacy were also confirmed by the selective knockout of the *EZH2* gene and its associated signaling molecules (Figure 6F).

Acquired resistance is a general phenomenon in chemotherapy and the efficacy of cisplatin-based chemotherapy in lung cancer is limited by the occurrence of innate and acquired drug resistance. Therefore, identifying the relevant resistance mechanisms operating in the presence of cisplatin in lung cancer cells can improve the clinical efficacy of targeted cancer drugs. It has been shown that *EZH2* is involved in cisplatin resistance in cancers (45). We observed an enhanced expression of miR-21 and *EZH2* with an increasing time of cisplatin treatment in lung cancer cells (Figure 6G, H, and Supplementary Figure S7). Combinatorial treatment of *EZH2*-targeting CRISPR Self *Check-In* with cisplatin enhanced therapeutic efficacy in the cancer cells (Figure 6I). Finally, we tested any synergistic effect of cisplatin treatment with *EZH2* suppression by CRISPR Self *Check-In* for lung cancer treatment. The combinatorial treatment of cisplatin and *EZH2*-targeting CRISPR Self *Check-In* showed a synergistic anti-tumour effect *in vivo* (Figure 6J–L). Interestingly, an enhanced expression of *EZH2* was observed in the cisplatin treatment group, which explained the mechanism underlying the synergistic effect of the combinatorial treatment of cisplatin and the CRISPR Self *Check-In* system (Figure 6L–P). Taken together, we demonstrated the potential of

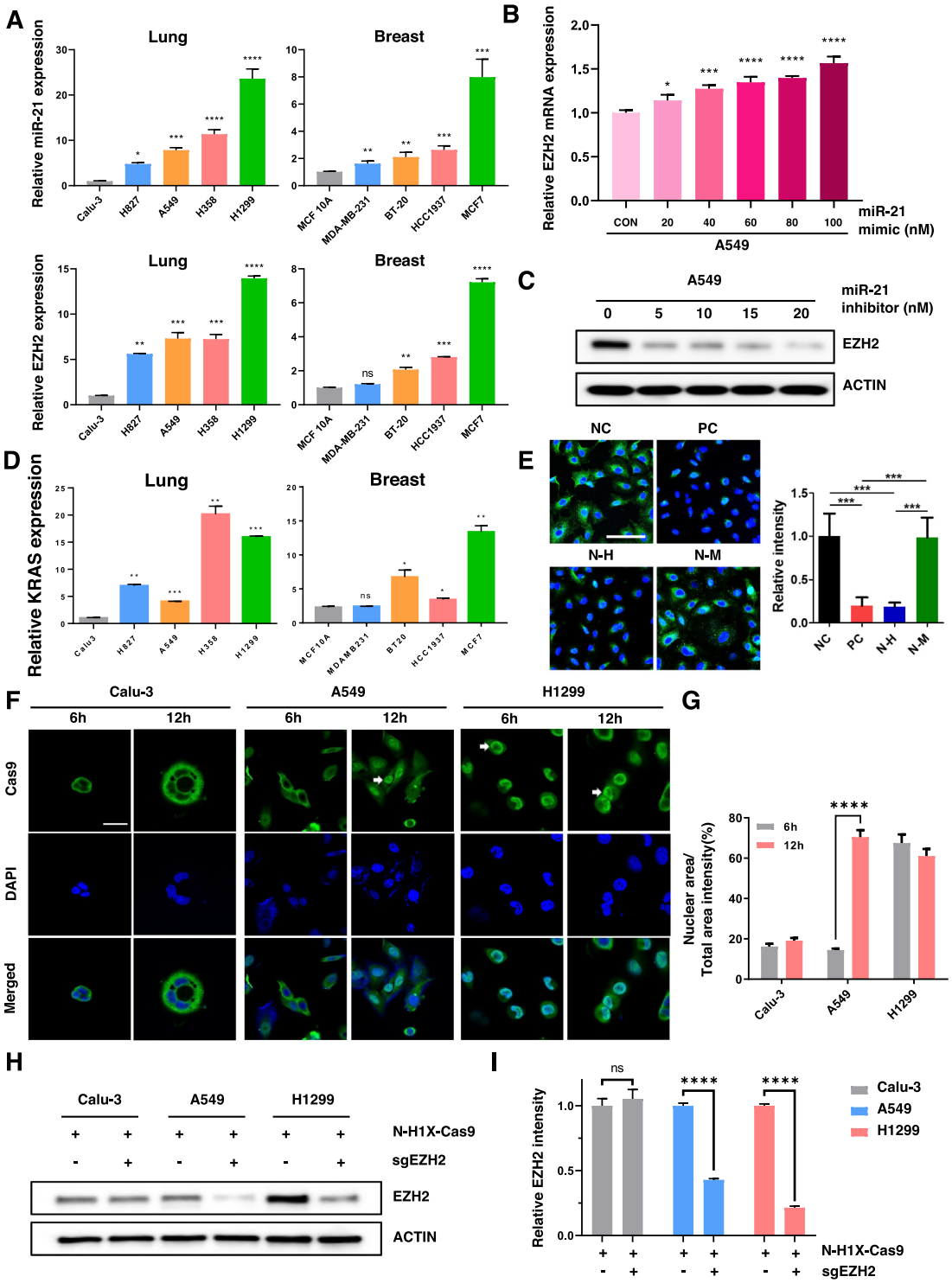

Figure 5. mRNA bridge mimetics as a novel switch platform for controlled gene editing of CRISPR Self *Check-In*. (**A**) MiR-21 and EZH2 mRNA expression in human cancer cell lines. (**B**) Increased mRNA expression of EZH2 with the treatment of increasing conc. of miR-21 mimic in A549 cells. (**C**) Decreased EZH2 protein level with the treatment of increasing conc. of miR-21 inhibitor in A549 cells. (**D**) KRAS mRNA expression in human cancer cell lines. (**E**) Immunofluorescence staining showing miRNA-21 specific k/o of KRAS using CRISPR Self *Check-In* targeting miR-21-KRAS axis in A549 cells. (**F**) Different patterns of N-H1X conjugated Cas9 translocation to the nucleus in Calu-3, A549, and H1299 cells were detected under observations after 6 and 12 h. Arrows indicate the translocation of Cas9 into the nucleus. (**G**) Quantification of detected translocation of Cas9 into the nucleus in (F). Bars indicated 50 μm. (**H**) WB for Knock-out of *EZH2* by CRISPR Self *Check-In* in miRNA conc. dependent manner. (**I**) Quantification of *EZH2* signal intensity normalized by actin in (G). All experiments in the present study were performed in triplicate. Error bars represent SD over biological replicates. *P* values were obtained using One-way ANOVA and unpaired Student's t-test. ns; no statistical significance, $*P < 0.05$, $**P < 0.01$, $***P < 0.001$ and $****P < 0.0001$.

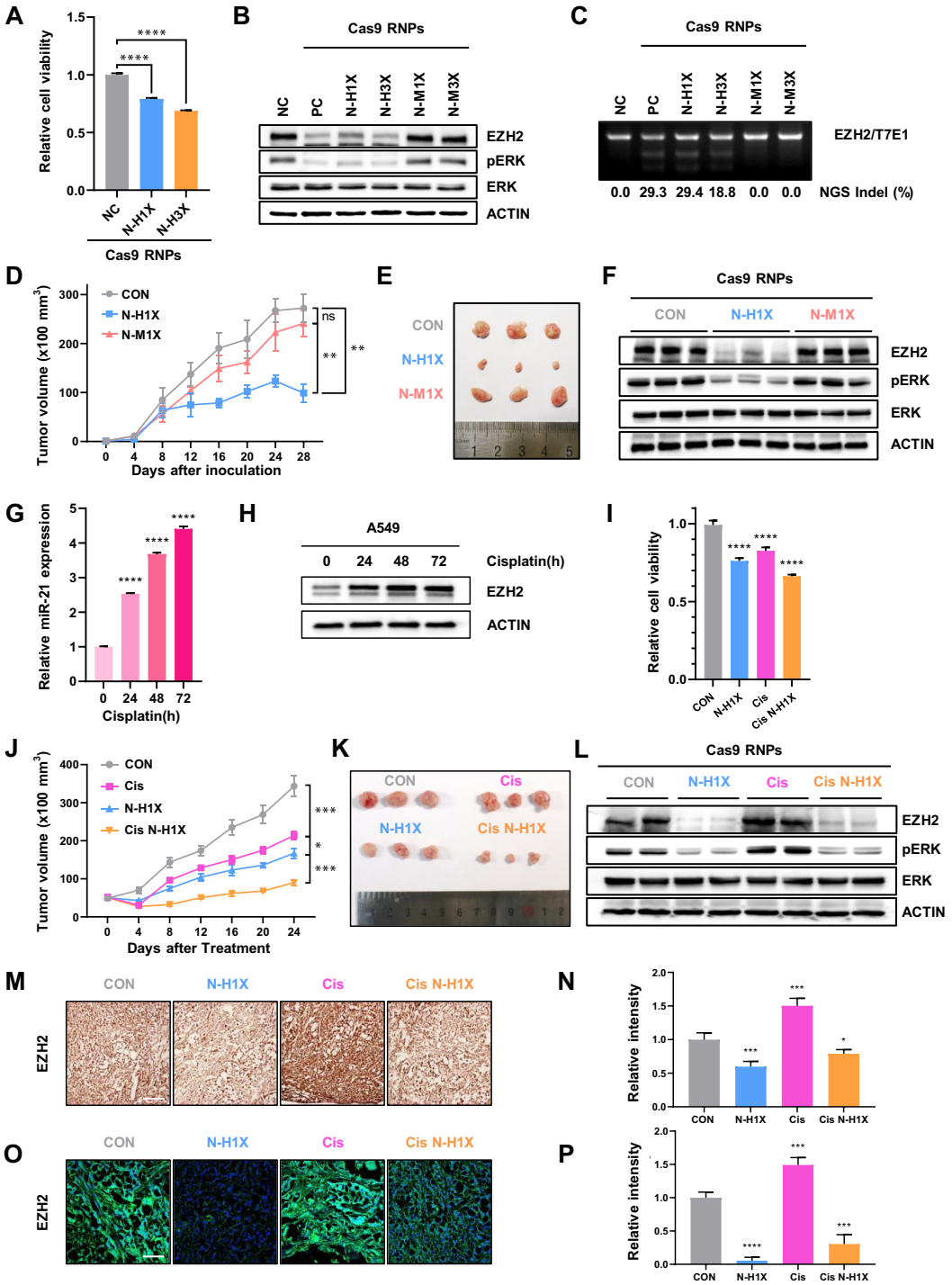

Figure 6. The potential of mRNA bridge mimetics in therapeutic applications. (**A** and **B**) The CRISPR Self *Check-In* targeting *EZH2* decreased human A549 cell viability after 72 h of transfection *in vitro*. The cell viability was decreased through inhibition of the ERK signaling pathway by *EZH2* knock-out. (**C**) T7E1 analysis shows the controlled genome editing by CRISPR Self *Check-In in vitro*. Indel frequency was measured by Targeted Deep Sequencing. (**D** and **E**) The decreased tumorigenic potential via selective gene editing was confirmed at 28 days after the inoculation of A549 cells transfected by CRISPR Self *Check-In* targeting *EZH2 in vivo*. (**F**) WB for *EZH2* knockout by CRISPR Self *Check-In in vivo* shown in D and E (**G**) Increase of miR-21 expression by cisplatin treatment (10 μM) in A549 cells. (**H**) Increase of *EZH2* expression by cisplatin treatment (10 μM) in A549 cells. (**I**) Combinatorial treatment of cisplatin (10 μM) and CRISPR Self *Check-In* targeting *EZH2* enhances anti-cancer efficacy in A549 cells after 72 h of transfection *in vitro*. (**J** and **K**) Combinatorial treatment of cisplatin with CRISPR Self *Check-In* targeting *EZH2* after 2 weeks of A549 inoculation into the mouse increases anti-tumour efficacy *in vivo*. (**L**) WB for *EZH2* knockout by CRISPR Self *Check-In in vivo* shown in J and K (**M** and **N**) Decrease of enhanced EZH2 expression induced by cisplatin with CRISPR Self *Check-In* treatment *in vivo* shown by immunohistochemistry. Bars indicated 200 μm. (**O** and **P**) Immunofluorescence staining of EZH2. Green: EZH2, Blue: DAPI. Bars indicated 100 μm. All experiments in the present study were performed in triplicate. Error bars represent SD over biological replicates. *P* values were obtained using One-way ANOVA. ns; no statistical significance, $*P < 0.05$, $**P < 0.01$, $***P < 0.001$ and $****P < 0.0001$.

CRISPR Self *Check-In* as a new therapeutic platform for both controlled gene editing with enhanced safety and combinatorial therapy with existing therapeutics against lung cancers.

DISCUSSION

In this study, we successfully developed mRNA bridge mimetics as a switch platform to regulate the translocation of proteins and applied it to control the nucleus translocation of Cas9 protein, thereby exhibiting disease-specific, controlled genome modification. The mRNA bridge mimetics platform was capable of sensing a specific miRNA and being cleaved off by miRNA-Ago complexes. The programmability of the mRNA bridge mimetics was achieved when there was complete complementation between the miRNA and the customized oligonucleotide sequences in it. Cell and tissue-specific activation of Cas9 protein has been extensively explored for precise genome editing. While several methods that combine CRISPR RNP with extrinsic signals have been developed, the potential of the system to respond to disease-specific intrinsic signals has not been widely explored. Even though a few miRNA-responsive CRISPR-Cas platforms have been found, the regulation of CRISPR RNP is absent (46). The CRISPR Self *Check-In* system was designed such that the translocation of Cas9 protein was programmed by mRNA bridge mimetics. As the mRNA bridge mimetics contain the NES that inhibits nuclear localization of Cas9, it allows CRISPR Self *Check-In* to be activated for gene editing only after the cleavage of mRNA bridge mimetics in the cytoplasm. We also elucidated the underlying mechanism of CRISPR Self *Check-In* via molecular dynamics simulation by showing that miRNA-Ago complexes have access to the mRNA bridge mimetics, which are exposed on the outer surface of CRISPR Self *Check-In*. Finally, we proposed that the CRISPR Self *Check-In* may be used as an alternate strategy to currently available cisplatin-based therapies for lung cancers. The *EZH2*-targeting CRISPR Self *Check-In* showed significant synergistic anti-tumor efficacy with a low dose of cisplatin, demonstrating a new strategy for effective and precise lung cancer treatment.

Our platform is based on peptide-oligonucleotide conjugates that are molecular composites containing a nucleic acid moiety linked to a polypeptide moiety by click reaction. RNA and peptide conjugates have been constructed for various therapeutic applications such as the delivery of a siRNA-based drug (47) and the screening of peptide libraries in an mRNA display method (48). Because the step-by-step solid-phase synthesis of the conjugates faces difficulties in finding the compatible protecting groups for both nucleotide bases and amino-acid side chains, post-synthetic conjugations of the respective nucleotides and peptides are the general and reliable coupling method to construct peptide-oligonucleotide conjugates. NES conjugated mRNA bridge mimetics are open to being coupled to a variety of drug moieties including small peptide drugs compared to large Cas9 proteins. However, it would also be helpful for the drug delivery of our RNA-peptide or protein conjugates such as self-assembled scaffold based nanostructure or an efficient viral delivery system of functional RNP into the cell (49,50).

Exploiting the potential of a cell's natural biology may uncover novel approaches to treat diseases. Innate sensing-mediated regulatory tools such as mRNA bridge mimetics could provide new switch platforms for this purpose. CRISPR Self *Check-In* is one of the promising applications of mRNA bridge mimetics to overcome the off-target activities of CRISPR-Cas9. Although the coverage of our current platform is limited to cells expressing one specific miRNA or cells with elevated miRNA due to drug resistance, we suggest that our mRNA bridge mimetic platform is not restricted to a combination with Cas9, but can be applied to upregulate other transcription factors or co-regulators in the nucleus. However, substantial screening will be required for its application to specific conditions. By harnessing the innate mechanism of mRNA decay machinery, therapeutic agents other than CRISPR-Cas9, such as small molecules and peptides can also be selectively delivered. mRNA bridge mimetics may need further stability optimization for various applications. The mRNA bridge mimetics strategy is promising for applications in which the reaction must be controlled via intrinsic stimuli, and for Cas9 proteins to ensure precise genome modification in diseased conditions. Taken together, we demonstrate that the disease-specific translocation of Cas9 by naturally changed endogenous miRNA levels in cancer cells adds another layer to therapeutic applications of orchestrated heterogeneity in cancer. Our findings highlight the fact that miRNA biology may be employed for disease-specific regulation of target genes, and this technology may safely control the delivery of therapeutics in patients without a definite prior diagnosis of the disease.

DATA AVAILABILITY

The authors confirm that the data supporting the findings of this study are available within the article and the Supplementary Data.

SUPPLEMENTARY DATA

Supplementary Data are available at NAR Online.

ACKNOWLEDGEMENTS

The figures were generated using BioRender with a paid license to publish.

Authors contributions: C.S. designed the study, performed experiments, analyzed data, and wrote the manuscript. S.C.P., I.P., and H.K. performed experiments. C.L. performed experiments and analyzed Seq data. S.K. provided conceptual advice and field-specific expertise. J.Y.L. designed the study, analysed data, and wrote the manuscript. J.M.L. designed and supervised the study and wrote the manuscript. S.J.O. designed and supervised the study and wrote the manuscript. All authors approved the final version.

FUNDING

Samsung Research Funding & Incubation Center of Samsung Electronics [SRFC-MA2002-07] (to J.M.L.); Na-

tional Research Foundation (NRF) grant funded by the Korea government [2020R1C1C1009507]; KIST Institutional Program (to S.J.O.); NRF grant funded by the Korea government (MSIT) [2018R1C1B600543513, 2022R1C1C1005080 and 2020M3A9G710393 to J.Y.L.]. Funding for open access charge: Korea Institute of Science and Technology.
Conflict of interest statememt. None declared.

REFERENCES

1. Friedman,R.C., Farh,K.K., Burge,C.B. and Bartel,D.P. (2009) Most mammalian mRNAs are conserved targets of microRNAs. *Genome Res.*, **19**, 92–105.
2. Hammond,S.M., Boettcher,S., Caudy,A.A., Kobayashi,R. and Hannon,G.J. (2001) Argonaute2, a link between genetic and biochemical analyses of RNAi. *Science*, **293**, 1146–1150.
3. Wightman,B., Ha,I. and Ruvkun,G. (1993) Posttranscriptional regulation of the heterochronic gene lin-14 by lin-4 mediates temporal pattern formation in *C. elegans*. *Cell*, **75**, 855–862.
4. Landgraf,P., Rusu,M., Sheridan,R., Sewer,A., Iovino,N., Aravin,A., Pfeffer,S., Rice,A., Kamphorst,A.O., Landthaler,M. *et al.* (2007) A mammalian microRNA expression atlas based on small RNA library sequencing. *Cell*, **129**, 1401–1414.
5. Akram,F., Atique,N., Haq,I.U., Ahmed,Z., Jabbar,Z., Nawaz,A., Aqeel,A. and Akram,R. (2021) MicroRNA, a promising biomarker for breast and ovarian cancer: a review. *Curr. Protein Pept. Sci.*, **22**, 599–619.
6. Kabzinski,J., Maczynska,M. and Majsterek,I. (2021) MicroRNA as a novel biomarker in the diagnosis of head and neck cancer. *Biomolecules*, **11**, 844.
7. Wu,K.L., Tsai,Y.M., Lien,C.T., Kuo,P.L. and Hung,A.J. (2019) The roles of MicroRNA in lung cancer. *Int. J. Mol. Sci.*, **20**, 1611.
8. Wen,D., Danquah,M., Chaudhary,A.K. and Mahato,R.I. (2015) Small molecules targeting microRNA for cancer therapy: promises and obstacles. *J. Control. Release*, **219**, 237–247.
9. Zhang,S., Cheng,Z., Wang,Y. and Han,T. (2021) The risks of miRNA therapeutics: in a drug target perspective. *Drug Des Devel Ther*, **15**, 721–733.
10. Cong,L., Ran,F.A., Cox,D., Lin,S., Barretto,R., Habib,N., Hsu,P.D., Wu,X., Jiang,W., Marraffini,L.A. *et al.* (2013) Multiplex genome engineering using CRISPR/Cas systems. *Science*, **339**, 819–823.
11. Jinek,M., Chylinski,K., Fonfara,I., Hauer,M., Doudna,J.A. and Charpentier,E. (2012) A programmable dual-RNA-guided DNA endonuclease in adaptive bacterial immunity. *Science*, **337**, 816–821.
12. Mali,P., Yang,L., Esvelt,K.M., Aach,J., Guell,M., DiCarlo,J.E., Norville,J.E. and Church,G.M. (2013) RNA-guided human genome engineering via Cas9. *Science*, **339**, 823–826.
13. Wang,X.W., Hu,L.F., Hao,J., Liao,L.Q., Chiu,Y.T., Shi,M. and Wang,Y. (2019) A microRNA-inducible CRISPR-Cas9 platform serves as a microRNA sensor and cell-type-specific genome regulation tool. *Nat. Cell Biol.*, **21**, 522–530.
14. Park,H., Lee,G.R., Heo,L. and Seok,C. (2014) Protein loop modeling using a new hybrid energy function and its application to modeling in inaccurate structural environments. *PLoS One*, **9**, e113811.
15. Leman,J.K., Weitzner,B.D., Lewis,S.M., Adolf-Bryfogle,J., Alam,N., Alford,R.F., Aprahamian,M., Baker,D., Barlow,K.A., Barth,P. *et al.* (2020) Macromolecular modeling and design in Rosetta: recent methods and frameworks. *Nat. Methods*, **17**, 665–680.
16. Gruber,A.R., Bernhart,S.H. and Lorenz,R. (2015) The ViennaRNA web services. *Methods Mol. Biol.*, **1269**, 307–326.
17. Haberthur,U. and Caflisch,A. (2008) FACTS: fast analytical continuum treatment of solvation. *J. Comput. Chem.*, **29**, 701–715.
18. Brooks,B.R., Brooks,C.L. III, Mackerell,A.D. Jr, Nilsson,L., Petrella,R.J., Roux,B., Won,Y., Archontis,G., Bartels,C., Boresch,S. *et al.* (2009) CHARMM: the biomolecular simulation program. *J. Comput. Chem.*, **30**, 1545–1614.
19. Jo,S., Cheng,X., Lee,J., Kim,S., Park,S.J., Patel,D.S., Beaven,A.H., Lee,K.I., Rui,H., Park,S. *et al.* (2017) CHARMM-GUI 10 years for biomolecular modeling and simulation. *J. Comput. Chem.*, **38**, 1114–1124.
20. Pettersen,E.F., Goddard,T.D., Huang,C.C., Meng,E.C., Couch,G.S., Croll,T.I., Morris,J.H. and Ferrin,T.E. (2021) UCSF ChimeraX: structure visualization for researchers, educators, and developers. *Protein Sci.*, **30**, 70–82.
21. Gouda,H., Kuntz,I.D., Case,D.A. and Kollman,P.A. (2003) Free energy calculations for theophylline binding to an RNA aptamer: Comparison of MM-PBSA and thermodynamic integration methods. *Biopolymers*, **68**, 16–34.
22. Greenidge,P.A., Kramer,C., Mozziconacci,J.C. and Wolf,R.M. (2013) MM/GBSA binding energy prediction on the PDBbind data set: successes, failures, and directions for further improvement. *J. Chem. Inf. Model.*, **53**, 201–209.
23. Maier,J.A., Martinez,C., Kasavajhala,K., Wickstrom,L., Hauser,K.E. and Simmerling,C. (2015) ff14SB: improving the accuracy of protein side chain and backbone parameters from ff99SB. *J. Chem. Theory Comput.*, **11**, 3696–3713.
24. Zgarbova,M., Otyepka,M., Sponer,J., Mladek,A., Banas,P., Cheatham,T.E. III and Jurecka,P. (2011) Refinement of the Cornell et al. nucleic acids force field based on reference quantum chemical calculations of glycosidic torsion profiles. *J. Chem. Theory Comput.*, **7**, 2886–2902.
25. Jorgensen,W.L., Chandrasekhar,J. and Madura,J.D. (1983) Comparison of simple potential functions for simulating liquid water. *J. Chem. Phys.*, **79**, 926.
26. Lee,T.S., Cerutti,D.S., Mermelstein,D., Lin,C., LeGrand,S., Giese,T.J., Roitberg,A., Case,D.A., Walker,R.C. and York,D.M. (2018) GPU-Accelerated molecular dynamics and free energy methods in Amber18: Performance enhancements and new features. *J. Chem. Inf. Model.*, **58**, 2043–2050.
27. Case,D.A., Belfon,H.M.A.K., Ben-Shalom,I.Y., Brozell,S.R., Cerutti,D.S., Cheatham,T.E. III, Cisneros,G.A., Darden,V.W.D.C.T.A., Duke,R.E., Giambasu,G. *et al.* (2020) AMBER 2020.
28. Miller,B.R. III, McGee,T.D. Jr, Swails,J.M., Homeyer,N., Gohlke,H. and Roitberg,A.E. (2012) MMPBSA.py: An efficient program for end-state free energy calculations. *J. Chem. Theory Comput.*, **8**, 3314–3321.
29. Onufriev,A., Bashford,D. and Case,D.A. (2004) Exploring protein native states and large-scale conformational changes with a modified generalized born model. *Proteins*, **55**, 383–394.
30. Shin,C.H., Byun,J., Lee,K., Kim,B., Noh,Y.K., Tran,N.L., Park,K., Kim,S.H., Kim,T.H. and Oh,S.J. (2020) Exosomal miRNA-19a and miRNA-614 induced by air pollutants promote proinflammatory M1 macrophage polarization via regulation of RORalpha expression in human respiratory mucosal microenvironment. *J. Immunol.*, **205**, 3179–3190.
31. Kim,S.M., Shin,S.C., Kim,E.E., Kim,S.H., Park,K., Oh,S.J. and Jang,M. (2018) Simple in vivo gene editing via direct self-assembly of Cas9 ribonucleoprotein complexes for cancer treatment. *ACS Nano*, **12**, 7750–7760.
32. Yu,X., Liang,X., Xie,H., Kumar,S., Ravinder,N., Potter,J., de Mollerat du Jeu,X. and Chesnut,J.D. (2016) Improved delivery of Cas9 protein/gRNA complexes using lipofectamine CRISPRMAX. *Biotechnol. Lett.*, **38**, 919–929.
33. Shin,C.H., Lee,M.G., Han,J., Jeong,S.I., Ryu,B.K. and Chi,S.G. (2017) Identification of XAF1-MT2A mutual antagonism as a molecular switch in cell-fate decisions under stressful conditions. *Proc. Natl. Acad. Sci. U.S.A.*, **114**, 5683–5688.
34. Park,J., Lim,K., Kim,J.S. and Bae,S. (2017) Cas-analyzer: an online tool for assessing genome editing results using NGS data. *Bioinformatics*, **33**, 286–288.
35. Dai,L., Chen,F., Zheng,Y., Zhang,D., Qian,B., Ji,H., Long,F. and Cretoiu,D. (2019) miR-21 regulates growth and EMT in lung cancer cells via PTEN/Akt/GSK3beta signaling. *Front. Biosci. (Landmark Ed.)*, **24**, 1426–1439.
36. Liu,Z., Yu,M., Fei,B., Fang,X., Ma,T. and Wang,D. (2018) miR215p targets PDHA1 to regulate glycolysis and cancer progression in gastric cancer. *Oncol. Rep.*, **40**, 2955–2963.
37. Shi,L., Middleton,J., Jeon,Y.J., Magee,P., Veneziano,D., Lagana,A., Leong,H.S., Sahoo,S., Fassan,M., Booton,R. *et al.* (2018) KRAS induces lung tumorigenesis through microRNAs modulation. *Cell Death. Dis.*, **9**, 219.
38. Wang,H., Tan,Z., Hu,H., Liu,H., Wu,T., Zheng,C., Wang,X., Luo,Z., Wang,J., Liu,S. *et al.* (2019) microRNA-21 promotes breast cancer

proliferation and metastasis by targeting LZTFL1. *BMC Cancer*, **19**, 738.
39. Xia,H., Zhang,W., Zhang,B., Zhao,Y., Zhao,Y., Li,S. and Liu,Y. (2017) miR-21 modulates the effect of EZH2 on the biological behavior of human lung cancer stem cells in vitro. *Oncotarget*, **8**, 85442–85451.
40. Zhao,Q., Chen,S., Zhu,Z., Yu,L., Ren,Y., Jiang,M., Weng,J. and Li,B. (2018) miR-21 promotes EGF-induced pancreatic cancer cell proliferation by targeting Spry2. *Cell Death. Dis.*, **9**, 1157.
41. Gong,J., Wu,Y., Zhang,X., Liao,Y., Sibanda,V.L., Liu,W. and Guo,A.Y. (2014) Comprehensive analysis of human small RNA sequencing data provides insights into expression profiles and miRNA editing. *RNA Biol*, **11**, 1375–1385.
42. Chen,F., Sun,H., Wang,J., Zhu,F., Liu,H., Wang,Z., Lei,T., Li,Y. and Hou,T. (2018) Assessing the performance of MM/PBSA and MM/GBSA methods. 8. Predicting binding free energies and poses of protein-RNA complexes. *RNA*, **24**, 1183–1194.
43. Fujii,S., Tokita,K., Wada,N., Ito,K., Yamauchi,C., Ito,Y. and Ochiai,A. (2011) MEK-ERK pathway regulates EZH2 overexpression in association with aggressive breast cancer subtypes. *Oncogene*, **30**, 4118–4128.
44. Hatley,M.E., Patrick,D.M., Garcia,M.R., Richardson,J.A., Bassel-Duby,R., van Rooij,E. and Olson,E.N. (2010) Modulation of K-Ras-dependent lung tumorigenesis by MicroRNA-21. *Cancer Cell*, **18**, 282–293.
45. Hu,S., Yu,L., Li,Z., Shen,Y., Wang,J., Cai,J., Xiao,L. and Wang,Z. (2010) Overexpression of EZH2 contributes to acquired cisplatin resistance in ovarian cancer cells in vitro and in vivo. *Cancer Biol. Ther.*, **10**, 788–795.
46. Hirosawa,M., Fujita,Y., Parr,C.J.C., Hayashi,K., Kashida,S., Hotta,A., Woltjen,K. and Saito,H. (2017) Cell-type-specific genome editing with a microRNA-responsive CRISPR-Cas9 switch. *Nucleic Acids Res.*, **45**, e118.
47. Tai,W. and Gao,X. (2017) Functional peptides for siRNA delivery. *Adv. Drug. Deliv. Rev.*, **110-111**, 157–168.
48. Wilson,D.S., Keefe,A.D. and Szostak,J.W. (2001) The use of mRNA display to select high-affinity protein-binding peptides. *Proc. Natl. Acad. Sci. U.S.A.*, **98**, 3750–3755.
49. Hayashi,H., Kubo,Y., Izumida,M. and Matsuyama,T. (2020) Efficient viral delivery of Cas9 into human safe harbor. *Sci. Rep.*, **10**, 21474.
50. Liu,Z., Cao,S., Liu,M., Kang,W. and Xia,J. (2019) Self-assembled multienzyme nanostructures on synthetic protein scaffolds. *ACS Nano*, **13**, 11343–11352.